Quantum State-Resolved Probing of Strong-Field-Ionized Xenon Atoms Using Femtosecond High-Order Harmonic Transient Absorption Spectroscopy

Zhi-Heng Loh,[1] Munira Khalil,[1] Raoul E. Correa,[1] Robin Santra,[2] Christian Buth,[2] and Stephen R. Leone[1,*]

[1]*Departments of Chemistry and Physics, University of California, Berkeley, California 94720, USA, and Chemical Sciences Division, Lawrence Berkeley National Laboratory, Berkeley, California 94720, USA*

[2]*Argonne National Laboratory, Argonne, Illinois 60439, USA*

(Received 19 January 2007; published 5 April 2007)

Femtosecond high-order harmonic transient absorption spectroscopy is used to resolve the complete $|j, m\rangle$ quantum state distribution of Xe^+ produced by optical strong-field ionization of Xe atoms at 800 nm. Probing at the Xe $N_{4/5}$ edge yields a population distribution $\rho_{j,|m|}$ of $\rho_{3/2,1/2}$:$\rho_{1/2,1/2}$:$\rho_{3/2,3/2} = 75 \pm 6 : 12 \pm 3 : 13 \pm 6\%$. The result is compared to a tunnel ionization calculation with the inclusion of spin-orbit coupling, revealing nonadiabatic ionization behavior. The sub-50-fs time resolution paves the way for tabletop extreme ultraviolet absorption probing of ultrafast dynamics.

DOI: 10.1103/PhysRevLett.98.143601 PACS numbers: 42.50.Hz, 32.80.Rm, 42.65.Ky, 82.53.−k

Studies of laser-atom interactions in the nonperturbative, strong-field regime elucidate novel phenomena such as above-threshold ionization [1,2], nonsequential double ionization [3], and high-order harmonic generation [4–6]. While these processes are extensively studied both experimentally and theoretically, details remain unknown about the $|j, m\rangle$ state distribution of the photoion produced by the initial photoionization step (m is the projection quantum number associated with the total angular momentum j of the hole). Moreover, experimental tests of theoretical models for strong-field ionization mostly rely on measuring the ion yield as a function of laser peak intensity [7]. The strong dependence of ionization yields on the orbital angular momentum and its direction relative to the laser polarization axis, as predicted by most theoretical models (e.g., the Ammosov-Delone-Krainov rates [8]), suggests that knowledge of the complete $|j, m\rangle$ state distribution can be used as an additional benchmark for theory. Young *et al.* recently reported the use of synchrotron x-ray pulses to probe the hole-orbital alignment of Kr^+ photoions generated in the strong-field ionization of Kr [9]. The unresolved fine-structure transitions prevented retrieval of the complete $|j, m\rangle$ state distribution. However, the observed degree of alignment is reproduced by the $|j, m\rangle$ state distribution obtained by tunnel ionization calculations with the inclusion of spin-orbit coupling [10].

Here we investigate the experimental and theoretical strong-field ionization of xenon to extract the complete $|j, m\rangle$ quantum state distribution. Femtosecond extreme ultraviolet (EUV) transient absorption spectroscopy is demonstrated with a laser-based, high-order harmonic probe source for the experiments; results are compared to tunnel ionization calculations that incorporate spin-orbit coupling. The resultant angular momentum distribution and hole-orbital alignment of the Xe^+ photoions are measured by probing the transition from the $4d$ core level to the $5p$ valence shell. These measurements allow the determination of the complete $|j, m\rangle$ quantum state distribution, which is compared to theory.

The schematic of the experimental setup is illustrated in Fig. 1. Briefly, the amplified output from a commercial Ti:sapphire laser system (2.4 W, 800 nm, 45 fs, 1 kHz) is sent to a 20:80 beam splitter to produce the optical pump and high-order harmonic generation beam, respectively. High-order harmonics in the EUV region are generated by focusing the laser light into a 7 cm long, 150 μm internal diameter capillary filled with 6.0×10^3 Pa of neon [11]. The estimated photon flux at the source is 10^4 photons per pulse for the high-order harmonic centered at 55.4 eV. A pair of 0.2 μm thick Al foils is used to reject the residual 800 nm light and transmit the high-order harmonics. After reflection by a toroidal mirror, the high-order harmonics are refocused into a 2 mm long gas cell filled with 2.7×10^3 Pa of Xe [12]. Scanning knife-edge measurements give a beam waist of 21 μm for the high-order harmonics. The transmitted EUV radiation is spectrally dispersed in a home-built spectrometer and detected with a thermoelectrically cooled CCD camera. A dielectric-coated mirror with a 1 mm diameter internal bore hole allows the optical pump beam to overlap with the EUV-probe beam in a collinear geometry. A half-wave plate

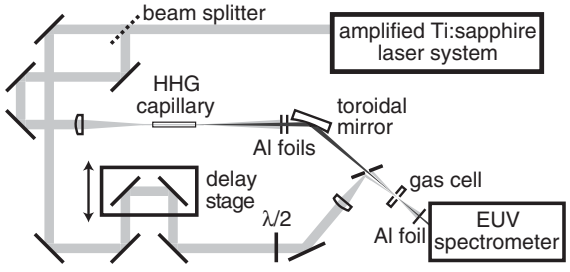

FIG. 1. Schematic illustration of the experimental setup. The light and dark lines correspond to the 800 nm pump and EUV-probe beam paths, respectively.

inserted into the path of the pump beam allows the relative polarization of the pump and probe beams to be varied. The polarization purity of the pump beam is characterized by an extinction ratio of >200:1. The 800 nm pump pulse energy incident on the gas cell is 0.13 mJ. Further measurements confirm that the pump pulse energy after the gas cell remains unchanged (by <3%) upon rotation of the half-wave plate. In the presence of the Xe gas, the pump pulse duration increases slightly to 49 fs and the elliptical focal spot of the pump beam is characterized by horizontal and vertical beam waists of 61 and 34 μm, respectively; these parameters yield a peak intensity of 8×10^{13} W/cm^2 for the pump pulse. The pump-probe time delay is varied by means of an optical delay line in the path of the pump beam. Transient absorption spectra are obtained by using spectra collected at -500 fs time delay as the reference [13]; a negative time delay implies that the probe pulse arrives at the sample before the pump pulse. Error bars reported below correspond to 95% confidence interval limits.

The transient absorption spectrum of Xe^+ acquired at a pump-probe time delay of +500 fs and a parallel relative polarization between pump and probe beams is shown in Fig. 2 [14]. The peaks at 55.4 and 56.1 eV correspond to the $5p_{3/2}^{-1}(^2P_{3/2}) \rightarrow 4d_{5/2}^{-1}(^2D_{5/2})$ and $5p_{1/2}^{-1}(^2P_{1/2}) \rightarrow 4d_{3/2}^{-1}(^2D_{3/2})$ transitions, respectively, in agreement with literature values [15] (nl_j^{-1} symbolizes a hole in the nl orbital with angular momentum j; the corresponding term symbol is given in parentheses). The ratio of the areas of the two fine-structure absorption lines, defined as $R = I^{\parallel}_{3/2\rightarrow 5/2}/I^{\parallel}_{1/2\rightarrow 3/2}$, is found to be $R = 6.5 \pm 1.1$. The time evolution of the Xe^+ $^2P_{3/2}$ state is followed by varying the pump-probe time delay while monitoring the transient absorption signal at 55.4 eV. The resultant time traces obtained for parallel and perpendicular relative polarizations between pump and probe beams are shown in Fig. 3. Fitting the time traces to a convolution of a step function with a Gaussian yields FWHM values of 37 ± 1 fs and 39 ± 2 fs for parallel and perpendicular relative polarizations, respectively. Note that the temporal signal corresponds to a cross correlation of the Xe^+ population growth with the EUV pulse [16]. From the polarization-dependent absorption at positive time delays ≥ 50 fs, the polarization anisotropy, defined as $r = (I^{\parallel}_{3/2\rightarrow 5/2} - I^{\perp}_{3/2\rightarrow 5/2})/(I^{\parallel}_{3/2\rightarrow 5/2} + 2I^{\perp}_{3/2\rightarrow 5/2})$, is found to be $r = 0.07 \pm 0.01$. The observed anisotropy implies the existence of hole-orbital alignment in the Xe^+ $^2P_{3/2}$ state produced by strong-field ionization. Since the hole orbital is directed along the polarization axis of the pump beam (which also defines the quantization axis), the hole population of the $m = \pm 1/2$ sublevels is expected to be greater than that of the $m = \pm 3/2$ sublevels, as observed experimentally. To verify the reliability of the measured polarization anisotropy, a separate set of measurements is performed for the $^2P_{1/2} \rightarrow {}^2D_{3/2}$ transition, for which no anisotropy is observed. This result agrees with the fact that alignment cannot exist in a $^2P_{1/2}$ state [17].

The experimental results for the ratio of the fine-structure absorption R and the polarization anisotropy r can be used to extract the complete quantum state distribution. The description of the EUV-probe step follows Ref. [10]. Let $\rho_{j,|m|}$ denote the probability of finding Xe^+ with a hole in either the $5p_{j,m}$ or the $5p_{j,-m}$ orbital. Making the dipole approximation and employing standard angular momentum algebra [17], we obtain

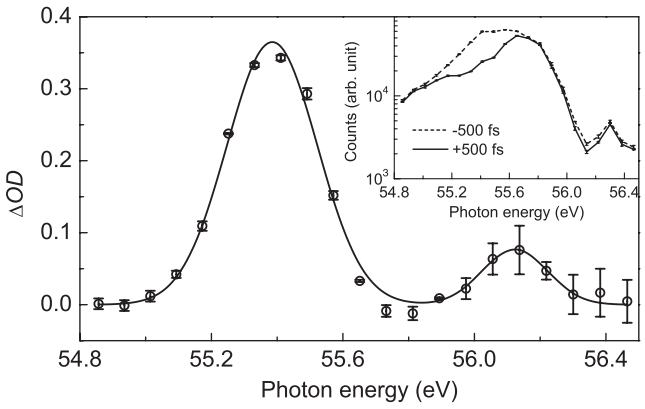

FIG. 2. Transient absorption spectrum of Xe^+ acquired at a time delay of +500 fs, obtained from the average of 3 data sets. ΔOD denotes the change in optical density (absorbance). The $^2P_{3/2} \rightarrow {}^2D_{5/2}$ and $^2P_{1/2} \rightarrow {}^2D_{3/2}$ fine-structure transitions are located at 55.4 and 56.1 eV, respectively. The fit to a sum of two Gaussian curves is depicted by the solid line. The inset shows the harmonic spectra obtained at -500 fs and +500 fs pump-probe time delay.

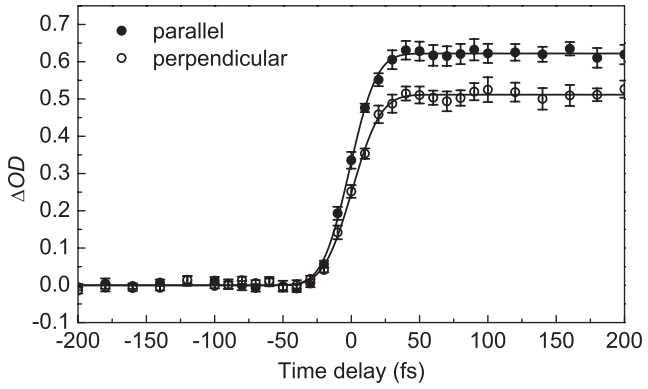

FIG. 3. Time evolution of the $^2P_{3/2} \rightarrow {}^2D_{5/2}$ transition for parallel and perpendicular relative polarizations between the optical pump and EUV-probe pulses, obtained from the average of 8 time scans for each relative polarization. The polarization anisotropy observed at positive time delays implies that the $^2P_{3/2}$ state of Xe^+ produced by strong-field ionization is aligned.

$$r = \frac{1}{10}\frac{\rho_{3/2,1/2} - \rho_{3/2,3/2}}{\rho_{3/2,1/2} + \rho_{3/2,3/2}} \quad (1)$$

and

$$R = \frac{3\rho_{3/2,1/2} + 2\rho_{3/2,3/2}}{5\rho_{1/2,1/2}}\,\xi, \quad (2)$$

where $\xi = |\langle {}^2D_{5/2} \parallel d \parallel {}^2P_{3/2}\rangle|^2/|\langle {}^2D_{3/2} \parallel d \parallel {}^2P_{1/2}\rangle|^2$ and d is the electric dipole operator. A multiconfiguration Dirac-Fock calculation performed with the program package GRASP2 [18] gives $\xi = 1.6$. From Eqs. (1) and (2), and the experimental values for R and r, the complete quantum state distribution of Xe^+ generated by strong-field ionization can be extracted. The results are summarized in Table I. We note that spectroscopic probing of the photoion by transient absorption allows direct retrieval of its quantum state distribution, which cannot be obtained from other experimental approaches to the study of strong-field ionization, such as energy- and angular-resolved photoelectron spectroscopy [19].

Tunnel ionization calculations with the inclusion of spin-orbit coupling are performed to model the experimental results described above. To calculate the production rates for the various ionization channels, the effective one-electron model described in Ref. [10] is employed. The model treats strong-field ionization within the tunneling picture and includes the effect of spin-orbit interaction. The approach makes use of a flexible finite-element basis set and determines ionization rates in this square-integrable basis using a complex absorbing potential [20]. Parameters that are used in the calculations are 0.13 mJ for the pulse energy, 49 fs FWHM for the pulse duration, and 45 μm for the cylindrically-symmetric beam waist. The $|j, m\rangle$ populations are calculated after the laser pulse by numerical integration of rate equations [10] and are normalized such that $\rho_{3/2,1/2} + \rho_{1/2,1/2} + \rho_{3/2,3/2} = 1$. The calculated fractional populations on the laser axis are shown in Table I. These calculations also allow us to verify that effects due to spatial averaging by the probe beam are smaller than the experimental errors for the $\rho_{j,|m|}$ distribution.

Within the given uncertainties, good agreement for the $\rho_{3/2,1/2}$:$\rho_{1/2,1/2}$ ratio is obtained between experiment and theory. This suggests that spin-orbit interaction is adequately treated in the tunnel ionization model employed in the calculations. Moreover, the calculations reveal that there is very little mixing between the $5p_{3/2}$ and $5p_{1/2}$ valence orbitals even at the saturation intensity for Xe^+ production. This implies that the laser field is not sufficiently strong to uncouple the spin-orbit interaction.

TABLE I. Comparison of the complete $|j, m\rangle$ quantum state distribution obtained from experiment and theory for Xe^+ generated via strong-field ionization.

$\lvert j, m\rangle$	Population distribution $\rho_{j,\lvert m\rvert}$(%) Experimental	Theoretical
$\lvert\frac{3}{2}, \pm\frac{1}{2}\rangle$	75 ± 6	83
$\lvert\frac{1}{2}, \pm\frac{1}{2}\rangle$	12 ± 3	14
$\lvert\frac{3}{2}, \pm\frac{3}{2}\rangle$	13 ± 6	3

Furthermore, the tunneling calculation predicts that $\rho_{3/2,3/2} \ll \rho_{3/2,1/2}$, which supports the experimental observation that the Xe^+ $^2P_{3/2}$ state produced by strong-field ionization is aligned. However, it is notable that the measured $\rho_{3/2,3/2}$:$\rho_{3/2,1/2}$ ratio of 0.17 ± 0.09 is significantly larger than that predicted by the calculation, which gives a value of 0.04 for this ratio. The discrepancy between experiment and theory can be attributed to the partial breakdown of the adiabatic (quasistatic) approximation employed in the tunnel ionization model.

The adiabatic approximation requires that the electrons within the atomic potential and those undergoing tunnel ionization respond instantaneously to the laser field. This approximation is analogous to the Born-Oppenheimer approximation frequently invoked in the study of molecular dynamics, whereby electrons are assumed to respond instantaneously to the electric field exerted by the nuclei. The ratio of the tunneling time to the period of the laser field is given by the Keldysh adiabaticity parameter γ [21], implying that the adiabatic approximation is valid only when $\gamma \ll 1$. Given that the experimental conditions yield $\gamma = \sqrt{I_p/2U_p} \sim 1.1$ (I_p is the atomic ionization potential and U_p is the ponderomotive potential), such a quasistatic approximation is no longer wholly valid; i.e., ionization becomes nonadiabatic with respect to the laser field. Under such circumstances, a nonperturbative multiphoton Floquet treatment of strong-field ionization becomes necessary [22]. Indeed, previous investigations of Xe strong-field ionization revealed discrete peaks atop above-threshold ionization features in the photoelectron spectra, suggesting that ionization occurs mainly via a multiphoton pathway [23,24]; the discrete peaks originate from resonance-enhanced multiphoton ionization that occurs when the field-dressed ground state crosses the ac Stark-shifted Rydberg states [25]. On the subcycle time scale, nonadiabatic transitions can occur between the field-dressed ground state and the Rydberg levels while varying the instantaneous phase of the laser field, akin to transitions between adiabatic potential energy surfaces in the non-Born-Oppenheimer regime of molecular dynamics. Note that nonadiabatic electron dynamics have previously been observed in molecular strong-field ionization, in which the spatial delocalization of electrons leads to the breakdown of the adiabatic approximation [26].

In the present work, the importance of nonadiabatic effects in atomic strong-field ionization is substantiated by the results of two spin-orbit-free calculations—a tunneling calculation and a multiphoton Floquet-type calculation [27]—performed at an intensity of 8×10^{13} W/cm^2.

The Floquet calculation predicts that the ratio of the $m_l = \pm 1 : m_l = 0$ ionization rates is $\sim 2\times$ larger than that predicted by the tunnel ionization model. Therefore it is reasonable that the experimentally measured $\rho_{3/2,3/2}$:$\rho_{3/2,1/2}$ ratio is larger than that predicted by the tunneling calculation with spin-orbit coupling. A valid theoretical comparison with the experimental result would require a Floquet calculation that incorporates spin-orbit coupling.

Finally, we note that while recent advances in high-order harmonic generation have already resulted in the extension of ultrafast spectroscopy into the EUV domain [28–31], most of the experiments reported to date have focused on photoelectron spectroscopy due to the set of discrete harmonics that presents itself as an attractive photoionization source. By probing transitions from the core level to unoccupied valence levels, picosecond time-resolved x-ray absorption near-edge spectroscopy based on laser-produced plasma [32] and synchrotron [33,34] sources have been shown to be highly sensitive to element-specific electronic structure changes accompanying photophysical and photochemical transformation. The work here demonstrates the feasibility of performing transient absorption spectroscopy with sub-50-fs time resolution using a laser-based, high-order harmonic source for core-level probing. Work on extending this technique to the study of ultrafast molecular dynamics is currently in progress.

We thank T. Pfeifer for useful discussions. The assistance from A. Paul and Professors M. M. Murnane and H. C. Kapteyn with implementing the HHG setup is gratefully acknowledged. This work was supported by the NSF ERC for EUV Science and Technology (No. EEC-0310717) and the LDRD program at LBNL, with additional equipment and support from DOE (No. DE-AC02-05CH11231). R. S. was supported by DOE (No. DE-AC02-06CH11357). C. B. was funded by the Alexander von Humboldt Foundation.

*Electronic address: srl@berkeley.edu

[1] P. Agostini *et al.*, Phys. Rev. Lett. **42**, 1127 (1979).
[2] P. B. Corkum, N. H. Burnett, and F. Brunel, Phys. Rev. Lett. **62**, 1259 (1989).
[3] B. Walker *et al.*, Phys. Rev. Lett. **73**, 1227 (1994).
[4] A. McPherson *et al.*, J. Opt. Soc. Am. B **4**, 595 (1987).
[5] A. L'Huillier and Ph. Balcou, Phys. Rev. Lett. **70**, 774 (1993).
[6] J. J. Macklin, J. D. Kmetec, and C. L. Gordon, Phys. Rev. Lett. **70**, 766 (1993).
[7] S. Augst *et al.*, J. Opt. Soc. Am. B **8**, 858 (1991).
[8] M. V. Ammosov, N. D. Delone, and V. P. Krainov, Sov. Phys. JETP **64**, 1191 (1986).
[9] L. Young *et al.*, Phys. Rev. Lett. **97**, 083601 (2006).
[10] R. Santra, R. W. Dunford, and L. Young, Phys. Rev. A **74**, 043403 (2006).
[11] A. Rundquist *et al.*, Science **280**, 1412 (1998).
[12] From the estimated electron rms velocity (1 μm/ps, corresponding to an electron temperature of $\sim$10 eV for the plasma) and typical electron-ion scattering cross sections ($\sim 10^{-16}$ cm^2), the time interval between each electron-ion collision event for the given sample density is $\sim$100 ps. Since this time is much longer than the maximum pump-probe time delay employed in the experiments, the observed dynamics are those of single ions, and the measured alignment distribution is not affected by electron-ion or ion-ion collisions.
[13] A constant background offset due to stray pump beam light incident on the CCD camera precludes the use of the pump-off spectrum as the reference spectrum.
[14] The minimum at 56.1 eV in the harmonic spectrum collected at -500 fs time delay exists in the weak continuum underlying the discrete harmonic peaks (note the use of a log scale); this could result from quantum interferences and macroscopic phase matching effects in HHG.
[15] P. Andersen *et al.*, J. Phys. B **34**, 2009 (2001).
[16] From the measured rise times and the computed time-evolution of $\rho_{3/2,1/2}$ and $\rho_{3/2,3/2}$, the EUV-probe pulse duration is estimated to be $\sim$30 fs.
[17] A. R. Edmonds, *Angular Momentum in Quantum Mechanics* (Princeton University, Princeton, New Jersey, 1996).
[18] F. A. Parpia, C. Froese-Fischer, and I. P. Grant, Comput. Phys. Commun. **94**, 249 (1996).
[19] B. Sheehy and L. F. DiMauro, Annu. Rev. Phys. Chem. **47**, 463 (1996).
[20] U. V. Riss and H.-D. Meyer, J. Phys. B **26**, 4503 (1993).
[21] L. V. Keldysh, Sov. Phys. JETP **20**, 1307 (1965).
[22] Note that the Floquet treatment, which is exact for a cw laser field, yields in the quasistatic limit the tunnel ionization model. The Floquet treatment itself is a cw limit to the solution of the time-dependent Schrödinger equation; the latter becomes necessary when the pulse envelope changes rapidly on the time scale of one laser cycle, as is the case for few-cycle pulses. For the 49-fs pulses used in this study, however, the Floquet treatment can be approximated as being exact.
[23] E. Mevel *et al.*, Phys. Rev. Lett. **70**, 406 (1993).
[24] B. Witzel, N. A. Papadogiannis, and D. Charalambidis, Phys. Rev. Lett. **85**, 2268 (2000).
[25] R. R. Freeman *et al.*, Phys. Rev. Lett. **59**, 1092 (1987).
[26] M. Lezius *et al.*, Phys. Rev. Lett. **86**, 51 (2001).
[27] C. Buth and R. Santra, Phys. Rev. A **75**, 033412 (2007).
[28] L. Nugent-Glandorf *et al.*, Phys. Rev. Lett. **87**, 193002 (2001).
[29] M. Bauer *et al.*, Phys. Rev. Lett. **87**, 025501 (2001).
[30] P. Siffalovic *et al.*, Rev. Sci. Instrum. **72**, 30 (2001).
[31] M. Drescher *et al.*, Nature (London) **419**, 803 (2002).
[32] F. Ráksi *et al.*, J. Chem. Phys. **104**, 6066 (1996).
[33] C. Bressler and M. Chergui, Chem. Rev. **104**, 1781 (2004).
[34] L. X. Chen, Annu. Rev. Phys. Chem. **56**, 221 (2005).